PAIRING CORRELATIONS AND THERMODYNAMIC PROPERTIES OF INNER CRUST MATTER

Jérôme Margueron, N. Sandulescu

HAL Id: in2p3-00659025
https://hal.in2p3.fr/in2p3-00659025

Submitted on 11 Jan 2012

Chapter 1

PAIRING CORRELATIONS AND THERMODYNAMIC PROPERTIES OF INNER CRUST MATTER

Jérôme Margueron[1][*] *and Nicolae Sandulescu*[2][†]

[1] Institut de Physique Nucléaire, IN2P3-CNRS and Université Paris-Sud,
F-91406 Orsay CEDEX, France

[2] Institute of Physics and Nuclear Engineering, 76900 Bucharest, Romania

January 13, 2012

Abstract

In this review paper we discuss the effects of pairing correlations on inner crust matter in the density region where nuclear clusters are supposed to coexist with non-localised neutrons. The pairing correlations are treated in the framework of the finite temperature Hartree-Fock-Bogoliubov approach and using zero range nuclear forces. After a short introduction and presentation of the formalism we discuss how the pairing correlations affect the structure of the inner crust matter, i.e., the proton to neutron ratio and the size of Wigner-Seitz cells. Then we show how the pairing correlations influence, though the specific heat of neutrons, the thermalization of the crust in the case of a rapid cooling scenario.

[*]E-mail jerome.margueron@ipno.in2p3.fr
[†]E-mail sandulescu@theory.nipne.ro

1.   Introduction

The superfluid properties of the inner crust of neutron stars have been considered long ago in connection to the large relaxation times which follow the giant glitches. Thus, according to the present models, the glitches are supposed to be generated by the unpinning of the superfluid vortex lines from the nuclear clusters immersed in the inner crust of neutron stars [1, 47]. Later on the superfluidity of the inner crust matter was also considered in relation to the cooling of isolated neutron stars [34, 12] and, more recently, in the thermal after-burst relaxation of neutron stars from X-ray transients [56, 13, 29].

The superfluid properties of the inner crust are essentially determined by the non-localized neutrons. For baryonic densities smaller than about 1.4×10^{-14} g cm^{-3} the non-localized neutrons are supposed to coexist with nuclei-type clusters [11, 43]. At higher densities, before the nuclear matter becomes uniform, the neutrons and the protons can form other configurations such as rods, plates, tubes and bubbles [46].

A microscopic *ab initio* calculation of pairing in inner crust matter should take into account the polarization effects induced by the nuclear medium upon the bare nucleon-nucleon interaction. This is a very difficult task which is not yet completely solved even for the infinite neutron matter. Thus, compared to BCS calculations with bare nucleon-nucleon forces, most of variational or diagrammatic models predict for infinite matter a substantial reduction of the pairing correlations due to the in-medium polarisation effects [36]. On the other hand, calculations based on Monte Carlo techniques predict for dilute neutron matter results closer to the BCS calculations (for a recent study see [23]).

A consistent treatment of polarization effects on pairing is still missing for inner crust matter (for a recent exploratory study see [6]). Therefore at present the most advanced microscopic model applied to inner crust matter remains the Hartree-Fock-Bogoliubov (HFB) approach. Pairing correlations have been also considered in the Quasiparticle Random Phase Approximation (QRPA)(see Section 2.1 below) in relation to the collective modes in inner crust matter [31]. However, a systematic investigation of the effect of collective QRPA excitations on thermodynamic properties of inner crust matter is still missing.

The scope of this chapter is to show how the HFB approach can be used to investigate the effects of pairing correlations on inner crust matter properties. Hence, in the first part of the chapter we will discuss the influence of pairing, treated in HFB approach at zero temperature, on the structure of inner crust matter. Then, using the HFB approach at finite temperature, we will show how the pairing correlations affect the specific heat and the thermalization of the inner crust matter in the case of a rapid cooling scenario.

In the present study we will focus only to the region of the inner crust which is supposed to be formed by a bbc crystal lattice of nuclear clusters embedded in non-localized neutrons. The crystal lattice is divided in elementary cells which are treated in the Wigner-Seitz approximation.

2. Treatment of pairing in the inner crust of neutron stars

2.1. Finite-temperature Hartree-Fock-Bogoliubov approach

In this section we discuss the finite-temperature HFB approximation for a Wigner-Seitz cell which contains in its center a nuclear cluster surrounded by a neutron gas. The cell contains also relativistic electrons which are considered uniformly distributed.

In principle, the HFB equations should be solved by respecting the bbc symmetry of the inner crust lattice. However, imposing the exact lattice symmetry in microscopic models is a very difficult task (for approximative solutions to this problem see Refs. [18, 26] and the references therein). We therefore solve the HFB equations for a spherical WS cell, as commonly done in inner crust studies [43, 3]. Since we are interested to describe the thermodynamic properties of the inner crust matter, we present here the HFB approach at finite temperature.

The HFB equations for a spherical WS cells have the same form as for isolated atomic nuclei. Thus, for zero range pairing forces and spherical symmetry, the HFB equations at finite temperature are defined as [24],

$$
\begin{pmatrix} h_{T,q}(r) - \lambda_q & \Delta_{T,q}(r) \\ \Delta_{T,q}(r) & -h_{T,q}(r) + \lambda_q \end{pmatrix} \begin{pmatrix} U_{i,q}(r) \\ V_{i,q}(r) \end{pmatrix} = E_{i,q} \begin{pmatrix} U_{i,q}(r) \\ V_{i,q}(r) \end{pmatrix}, \qquad (1)
$$

where $E_{i,q}$ is the quasiparticle energy, $E_{i,q} = \sqrt{(e_{i,q} - \lambda_q)^2 + \Delta_{i,q}^2}$, $U_{i,q}(r)$ and $V_{i,q}(r)$ are the components of the HFB wave function and λ_q is the chemical potential ($q = n, p$ is the index for neutrons and protons) . The quantity $h_{T,q}(r)$ is the thermal averaged mean field hamiltonian and $\Delta_{T,q}(r)$ is the thermal averaged pairing field.

In a self-consistent HFB calculation based on a Skyrme-type force, as used in the present study, $h_{T,q}(r)$ and $\Delta_{T,q}(r)$ are expressed in terms of thermal averaged densities, i.e., particle density $\rho_{T,q}(r)$, kinetic energy density $\tau_{T,q}(r)$, spin density $J_{T,q}(r)$ and, respectively, pairing density $\kappa_{T,q}(r)$. The thermal averaged densities mentioned above are given by [53]:

$$
\rho_{T,q}(r) = \frac{1}{4\pi} \sum_i g_{i,q} \left[|V_{i,q}(r)|^2 (1 - f_{i,q}) + |U_{i,q}(r)|^2 f_{i,q} \right], \qquad (2)
$$

$$
\tau_{T,q}(r) = \frac{1}{4\pi} \sum_i g_{i,q} \left\{ \left[\left(\frac{dV_{i,q}(r)}{dr} - \frac{V_{i,q}(r)}{r} \right)^2 + \frac{l_{i,q}(l_{i,q}+1)}{r^2} V_{i,q}(r)^2 \right] (1 - f_{i,q}) \right.
$$
$$
\left. + \left[\left(\frac{dU_{i,q}(r)}{dr} - \frac{U_{i,q}(r)}{r} \right)^2 + \frac{l_{i,q}(l_{i,q}+1)}{r^2} U_{i,q}(r)^2 \right] f_{i,q} \right\}, \quad (3)
$$

$$
J_{T,q}(r) = \frac{1}{4\pi} \sum_i g_{i,q} \left(j_{i,q}(j_{i,q}+1) - l_{i,q}(l_{i,q}+1) - \frac{3}{4} \right)
$$
$$
\times \left(|V_{i,q}(r)|^2 (1 - f_{i,q}) + |U_{i,q}(r)|^2 f_{i,q} \right), \qquad (4)
$$

$$
\kappa_{T,q}(r) = \frac{1}{4\pi} \sum_i g_{i,q} U_{i,q}^*(r) V_{i,q}(r) (1 - 2 f_{i,q}), \qquad (5)
$$

where $f_{i,q} = [1 + \exp(E_{i,q}/T)]^{-1}$ is the Fermi-Dirac distribution of quasiparticles, T is the temperature expressed in energy units, and $g_{i,q} = 2 j_{i,q} + 1$ is the degeneracy of the state i

with angular momentum j_i. The summations in the equations above are over the spectrum of bound nucleons which form the nuclear cluster and of unbound neutrons which form the neutron gas. A constant density at the edge of the WS cell is obtained imposing Dirichlet-Von Neumann boundary conditions at the edge of the cell [43], i.e., all wave functions of even parity vanish and the derivatives of odd-parity wave functions vanish.

The nuclear mean field has the same expression in terms of densities as in finite nuclei [19]. However, for a WS cell the Coulomb mean field of protons has an additional contribution coming from the interaction of the protons with the electrons given by

$$u_{\text{Coul}}^{pe}(r) = -e^2 \int d^3 r' \, \rho_e(r') \frac{1}{|r - r'|}. \tag{6}$$

Assuming that the electrons are uniformly distributed inside the cell, with the density $\rho_e = 3Z/(4\pi R_{WS}^3)$, one gets

$$u_{\text{Coul}}^{pe}(r) = -2\pi e^2 \rho_e \left(R_{WS}^2 - \frac{1}{3} r^2 \right) = \frac{Ze^2}{2R_{WS}} \left(\left(\frac{r}{R_{WS}} \right)^2 - 3 \right) \tag{7}$$

It can be seen that inside the WS cell the contribution of the proton-electron interaction to the proton mean field is quadratic in the radial coordinate.

The pairing field is calculated with a zero range force of the following form

$$V_{\text{Pair},q}(\mathbf{r_i}, \mathbf{r_j}) = V_0 \, g_{\text{Pair},q}[\rho_{T,n}(\mathbf{r}), \rho_{T,p}(\mathbf{r})](1 - P_\sigma)\delta(\mathbf{r}_{ij}) \,, \tag{8}$$

where $P_\sigma = (1 + \hat{\sigma}_1 \cdot \hat{\sigma}_2)/2$ is the spin exchange operator. For this interaction the pairing field is given by

$$\Delta_{T,q}(r) = V_0 \, g_{\text{Pair},q}[\rho_{T,n}(\mathbf{r}), \rho_{T,p}(\mathbf{r})] \, \kappa_{T,q}(r). \tag{9}$$

In the calculations presented here we use two different functionals for $g_{\text{Pair},q}[\rho_{T,n}(\mathbf{r}), \rho_{T,p}(\mathbf{r})]$. The first one, called below isoscalar (IS) pairing force, depends only on the total baryonic density, $\rho_{T,B}(r) = \rho_{T,n}(r) + \rho_{T,p}(r)$. Its expression is given by

$$g_{\text{Pair},q}[\rho_{T,n}(\mathbf{r}), \rho_{T,p}(\mathbf{r})] = 1 - \eta \left(\frac{\rho_{T,B}(r)}{\rho_0} \right)^\alpha \,, \tag{10}$$

where ρ_0 is the saturation density of the nuclear matter. This effective pairing interaction is extensively used in nuclear structure calculations and it was also employed for describing pairing correlations in the inner crust of neutron stars [52, 53, 54, 40]. The parameters are chosen to reproduce in infinite neutron matter two pairing scenarii, i.e., corresponding to a maximum gap of about 3 MeV (strong pairing scenario, hereafter named ISS) and, respectively, to a maximum gap around 1 MeV (weak pairing scenario, called below ISW). These two pairing scenarii are simulated by two values of the pairing strength, i.e., $V_0 = \{-570, -430\}$ MeV fm^{-3}. The other parameters are taken the same for the strong and the weak pairing, i.e., $\alpha = 0.45$, $\eta = 0.7$ and $\rho_0 = 0.16$ fm^{-3}. The energy cut-off, necessary to cure the divergence associated to the zero range of the pairing force, is introduced through the factor $e^{-E_i/100}$ acting for $E_i > 20$ MeV, where E_i are the HFB quasiparticle energies.

The second pairing functional, referred below as isovector strong pairing (IVS), depends explicitly on neutron and proton densities and has the following form in the neutron
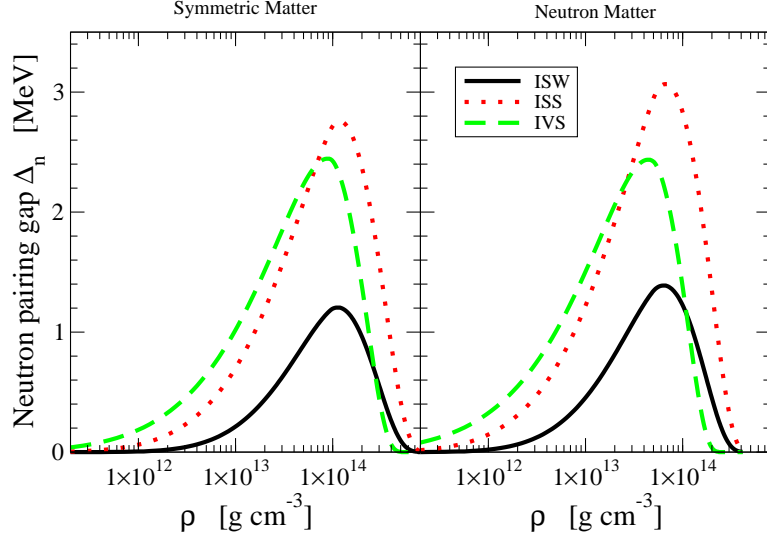
Figure 1. (color online) Neutron pairing gap for the interactions ISW (isoscalar weak), ISS (isoscalar strong) and IVS (isovector strong) in symmetric nuclear matter and in neutron matter.

channel [38],

$$g_{\mathrm{Pair},n}\big[\rho_{T,n}(\mathbf{r}), \rho_{T,p}(\mathbf{r})\big] = 1 - \eta_s(1-I(r))\left(\frac{\rho_{T,B}(r)}{\rho_0}\right)^{\alpha_s} - \eta_n I(r)\left(\frac{\rho_{T,B}(r)}{\rho_0}\right)^{\alpha_n} , \quad (11)$$

where $I(r) = \rho_{T,n}(r) - \rho_{T,p}(r)$. This interaction is adjusted to reproduce the neutron $^1S_0$ pairing gap in neutron and symmetric nuclear matter provided by the BCS calculations with the bare nucleon-nucleon forces [14]. In addition, the pairing strength V_0 and the cut-off energy are related to each other through the neutron-neutron scattering length according to the procedure described in Ref. [9]. Therefore this interaction is expected to describe properly the pairing for all the nuclear densities of the inner crust matter, including the low density neutron gas. As shown in Refs. [39, 10], this pairing functional describes well the two-neutron separation energies and the odd-even mass differences in nuclei with open shells in neutrons. In the present calculations for this pairing functional we have used the parameters V_0= -703.86 MeV fm^{-3}, η_s=0.7115, α_s=0.3865, η_n=0.9727, α_n=0.3906. The cut-off prescription is the same as for the isoscalar pairing force.

The pairing gaps in symmetric matter and neutron matter predicted by the three pairing forces introduced above are represented in Fig. 1 for a wide range of sub-nuclear densities. It can be seen that the isovector IVS interaction gives a maximum gap closer to the strong isoscalar ISS force, and the ISW interaction predict a suppression of the pairing gap up to saturation density.

To illustrate how the pairing correlations are spatially distributed in the Wigner-Seitz cells and how they are affected by the temperature, in Fig. 2 are shown the pairing fields for neutrons in the cells 2 and 5 (see Table 1). It can be noticed that the clusters have a non-trivial influence on the pairing of neutron gas. Thus, depending of the relative intensity of
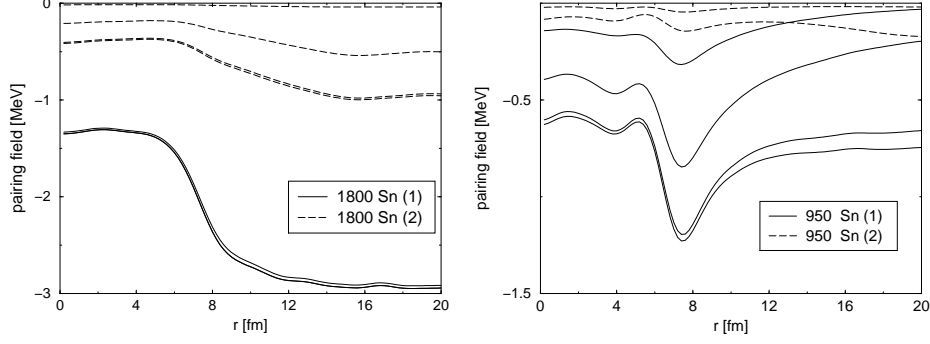
Figure 2. Neutron pairing fields for the Wigner-Seitz cells 2 and 5 (see Table 1) labeled, respectively, as ^{1800}Sn and ^{950}Sn. The full and the long-dashed lines correspond to the ISS and ISW pairing interaction. Here the calculations have been done with the strenghts $V_0 = \{-430, -330\}$ MeV fm^3 and with an energy cut-off of 60 MeV.

pairing in the cluster and the gas region, the presence of the cluster can suppress or enhance the pairing in the surface region of the cluster.

2.2. Quasiparticle Random Phase Approximation (QRPA)

Pairing correlations affect not only the ground state properties of inner crust matter but also its excitations modes. The non-collective excitations are commonly described by the quasiparticle energies obtained solving the HFB equations. To calculate the collective excitations one needs to take into account the residual interaction between the quasiparticles. In what follows we discuss briefly the collective modes of the inner crust matter in the framework of QRPA, which takes properly into account the pairing correlations [31].

The QRPA can be obtained from the time-dependent HFB approach in the limit of linear response. In the linear response theory the fundamental quantity is the Green function which satisfies the Bethe-Salpeter equation

$$\mathbf{G} = (\mathbf{1} - \mathbf{G_0 V})^{-1}\,\mathbf{G_0} = \mathbf{G_0} + \mathbf{G_0 V G}. \tag{12}$$

The unperturbed Green's function $\mathbf{G_0}$ has the form:

$$\mathbf{G_0}^{\alpha\beta}(\mathbf{r}\sigma, \mathbf{r}'\sigma'; \omega) = \sum_{ij} \frac{\mathcal{U}_{ij}^{\alpha 1}(\mathbf{r}\sigma)\bar{\mathcal{U}}_{ij}^{*\beta 1}(\mathbf{r}'\sigma')}{\hbar\omega - (E_i + E_j) + i\eta} - \frac{\mathcal{U}_{ij}^{\alpha 2}(\mathbf{r}\sigma)\bar{\mathcal{U}}_{ij}^{*\beta 2}(\mathbf{r}'\sigma')}{\hbar\omega + (E_i + E_j) + i\eta}, \tag{13}$$

where E_i are the HFB quasiparticle energies and $\mathcal{U}_{ij}$ are 3 by 2 matrices expressed in term of the two components of the HFB wave functions [32]. The $\sum$ symbol in the equation above indicates that the summation is taken over the bound and unbound quasiparticle states. The latter corresponds here to the non-localised neutrons in the WS cell.

$\mathbf{V}$ is the matrix of the residual interaction expressed in terms of the second derivatives of the HFB energy functional, namely:

$$\mathbf{V}^{\alpha\beta}(\mathbf{r}\sigma, \mathbf{r}'\sigma') = \frac{\partial^2 \mathcal{E}}{\partial\rho_\beta(\mathbf{r}'\sigma')\partial\rho_{\bar{\alpha}}(\mathbf{r}\sigma)}, \quad \alpha, \beta = 1, 2, 3. \tag{14}$$
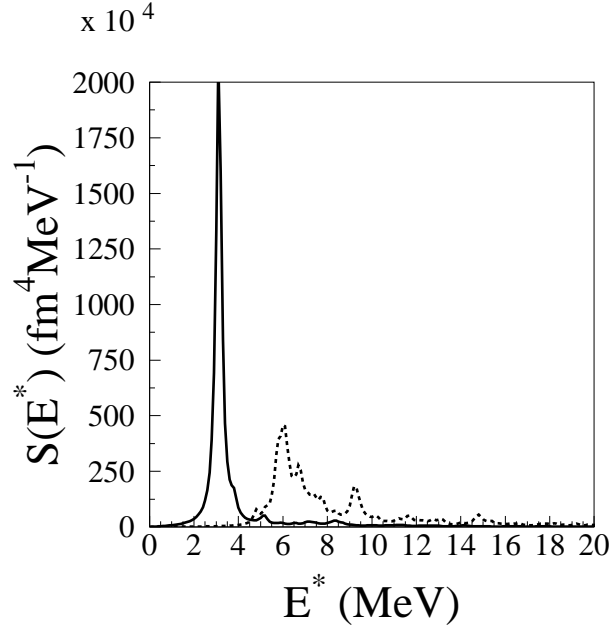
Figure 3. Strength distributions for the quadrupole mode in WS cell 2 of Table 1. The full (dashed) line corresponds to the QRPA (HFB) strength. The results are for ISS pairing force with the same parameters as used in Figure 1.

In the above equation $\{\rho_1, \rho_2, \rho_3\} \equiv \{\rho, \kappa, \kappa^*\}$, where ρ and κ are, respectively, the particle (2) and pairing (5) densities; the notation $\bar{\alpha}$ means that whenever α is 2 or 3 then $\bar{\alpha}$ is 3 or 2.

The linear response of the system to external perturbation is commonly described by the strength function. Thus, when the external perturbation is induced by a particle-hole external field F the strength function writes:

$$S(\omega) = -\frac{1}{\pi} Im \int F^*(\mathbf{r}) \mathbf{G}^{11}(\mathbf{r}, \mathbf{r}'; \omega) F(\mathbf{r}') d\mathbf{r} \; d\mathbf{r}' \tag{15}$$

where $\mathbf{G}^{11}$ is the (ph,ph) component of the QRPA Green's function.

As an example in Fig. 3 it is shown the strength function for the quadrupole response calculated for the WS cell 2 of Table 1 below [31]. The results correspond to the isoscalar pairing force with the strength V_0=-430 MeV fm^{-3} and an energy cut-off of 60 MeV. It can be seen that the unperturbed spectrum, distributed over a large energy region, becomes concentrated almost entirely in the peak located at about 3 MeV when the residual interaction between the quasiparticles is introduced. The peak collects more than 99% of the total quadrupole strength and it is extremely collective. An indication of the extreme collectivity of this low-energy mode can be also seen from its reduced transition probability, B(E2), which is equal to 25×10^3 Weisskopf units. This value of B(E2) is two orders of magnitude higher than in standard nuclei. This underlines the fact that in this WS cell the collective dynamics of the neutron gas dominates over the cluster contribution. In Ref. [31] it is shown that similar collective modes appears for the monopole and the dipole excitations. A very collective low-energy quadrupole mode it was also found in all the Wigner-Seitz cells with

N_{cell}	ρ_B [g cm^{-3}]	k_F [fm^{-1}]	N	Z	R_{WS} [fm]
1	$7.9\ 10^{13}$	1.12	1460	40	19.7
2	$3.4\ 10^{13}$	0.84	1750	50	27.7
3	$1.5\ 10^{13}$	0.64	1300	50	33.2
4	$9.6\ 10^{12}$	0.55	1050	50	35.8
5	$6.2\ 10^{12}$	0.48	900	50	39.4
6	$2.6\ 10^{12}$	0.36	460	40	42.3
7	$1.5\ 10^{12}$	0.30	280	40	44.4
8	$1.0\ 10^{12}$	0.26	210	40	46.5
9	$6.6\ 10^{11}$	0.23	160	40	49.4
10	$4.6\ 10^{11}$	0.20	140	40	53.8

Table 1. The structure of the Wigner-Seitz cells obtained from a density matrix expansion (DME) [43] ρ_B is the baryon density, $k_F = (3\pi^2 n_B)^{1/3}$ the Fermi momentum calculated as in Ref. [3] where n_B is the number of baryons per fm^3, N and Z are the numbers of neutrons and protons while R_{WS} is the radius of the WS cells. Compared to Ref. [43] here it is not shown the cell with the highest density located at the interface with the pasta phase.

Z=50 [27]. However, a systematic investigation of the influence of these collective modes on the thermodynamic properties of inner crust matter is still missing.

3.   The effect of pairing on inner crust structure

The first microscopic calculation of the inner-crust structure was performed by Negele and Vautherin in 1973 [43]. In this work the crystal lattice is divided in spherical cells which are treated in the Wigner-Seitz (WS) approximation. The nuclear matter from each cell is described in the framework of Hartree-Fock (HF) and the pairing is neglected. The properties of the WS cells found in Ref. [43], determined for a limited set of densities, are shown in Table I. The most remarkable result of this calculation is that the majority of the cells have semi-magic and magic proton numbers, i.e., Z=40,50. This indicates that in these calculations there are strong proton shell effects, as in isolated atomic nuclei.

The effect of pairing correlations on the structure of Wigner-Seitz cells was first investigated in Refs. [3, 4, 5] within the Hartree-Fock BCS (HFBCS) approach. In this section we shall discuss the results of a recent calculations based on Hartree-Fock-Bogoliubov approach [28]. This approach offers better grounds than HF+BCS approximation for treating pairing correlations in non-uniform nuclear matter with both bound and unbound neutrons.

As in Ref. [43], the lattice structure of the inner crust is described as a set of independent cells of spherical symmetry treated in the WS approximation. For baryonic densities below $\rho \approx 1.4 \times 10^{14}$ g/cm^3, each cell has in its center a nuclear cluster (bound protons and neutrons) surrounded by low-density and delocalized neutrons and immersed in a uniform gas of ultra-relativistic electrons which assure the charge neutrality. At a given baryonic density the structure of the cell, i.e., the N/Z ratio and the cell radius is determined from the minimization over N and Z of the total energy under the condition of beta equilibrium. The energy of the cell, relevant for determining the cell structure, has contributions from

the nuclear and the Coulomb interactions. Its expression is written in the following form

$$E = E_M + E_N + T_e + E_L. \tag{16}$$

The first term is the mass difference $E_M = Z(m_p + m_e) + (N - A)m_n$ where N and Z are the number of neutrons and protons in the cell and A=N+Z. E_N is the binding energy of the nucleons, which includes the contribution of proton-proton Coulomb interaction inside the nuclear cluster. T_e is the kinetic energy of the electrons while E_L is the lattice energy which takes into account the electron-electron and electron-proton interactions. The contribution to the total energy coming from the interaction between the WS cells [44] it is not considered since it is very small compared to the other terms of Eq.(1).

We shall now discuss the effect of pairing correlations on the structure of the WS cells. To study the influence of pairing correlations we have performed HFB calculations with the three pairing interactions introduced in Section 2.1.
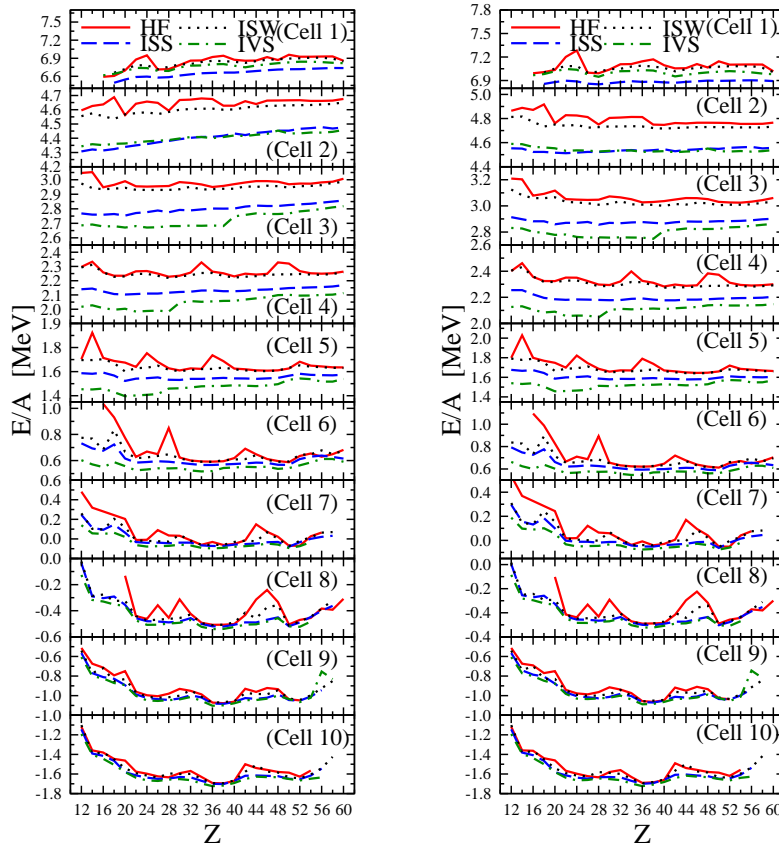

Figure 4. (color online) The HFB energies per particle as function of proton number for the pairing forces ISW (dotted line), ISS (dashed line) and IVS (dashed-dotted line). The solid lines represent the HF results. In the left pannel are shown the results obtained including the finite size corrections.

The structure of the WS cells obtained in the HFB approach is given in Table II while in Fig. 4 it is shown the dependence of the binding energies, at beta equilibrium, on protons

number. The contribution of pairing energy, nuclear energy and electron kinetic energy to the total energy are given in Fig. 5 for the cells 2 and 6. From this figure we can notice that the nuclear binding energy is almost compensated by the kinetic energy of the electrons which explains the weak dependence of the total energy on Z seen in Fig. 4. In Fig.4 we observe also that pairing is smoothing significantly the variation of the HF energy with Z. For this reason the HFB absolute minima are very little pronounced compared to the other neighboring energy values.

N_{cell}	N				Z				Z_{corr}			
	HF	ISW	ISS	IVS	HF	ISW	ISS	IVS	HF	ISW	ISS	IVS
2									40	40	22	42
3	318	514	442	554	16	24	20	24	54	40	28	38
4	476	534	382	570	28	28	20	28	40	40	40	28
5	752	320	328	344	46	20	20	20	46	48	44	20
6	454	428	374	346	50	48	36	34	50	50	50	34
7	316	344	324	240	50	50	50	36	50	50	50	50
8	174	220	186	174	36	50	38	36	36	50	38	36
9	120	112	128	116	38	36	38	36	38	36	38	36
10	94	82	90	82	38	36	38	36	36	36	36	36

Table 2. The structure of Wigner-Seitz cells obtained in the HF and HFB approximation. The results corresponds to the isoscalar weak (ISW), isoscalar strong (ISS) and isovector-isoscalar (IVS) pairing forces. In the last 4 columns are shown the proton numbers obtained with the finite size corrections. In the table are shown only the structures of the cells which could be well-defined by the present calculations.

From Fig. 4 we observe that in the cells 1-2 the binding energy does not converge to a minimum at low values of Z. For the cells 3-4, although absolute minima can be found for HF or/and HFB calculations, these minima are very close to the value of binding energy at the lowest values of Z we could explore. Therefore the structure of these cells is ambiguous. The situation is different in the cells 5-10 where the binding energies converge to absolute minima which are well below the energies of the configurations with the lowest Z values.

From Table II it can be observed that the structure of some cells becomes very different when the pairing is included. Moreover, these differences depend significantly on the intensity of pairing (see the results for ISW and ISS). However, as seen in Fig. 4, for the majority of cells the absolute minima are very little pronounced relative to the other energy values, especially for the HFB calculations. Therefore one cannot draw clear quantitative conclusions on how much pairing is changing the proton fraction in the cells.

When the radius of the cell becomes too small the boundary conditions imposed at the cell border through the WS approximation generate an artificial large distance between the energy levels of the nonlocalized neutrons. Consequently, the binding energy of the neutron gas is significantly underestimated. An estimation of how large could be the errors in the binding energy induced by the WS approximation can be obtained from the quantity

$$f(\rho_n, R_{WS}) \equiv B_{inf.}(\rho_n) - B_{WS-inf.}(\rho_n, R_{WS}) \,, \tag{17}$$

where the first term is the binding energy per neutron for infinite neutron matter of density ρ_n and the second term is the binding energy of neutron matter with the same density
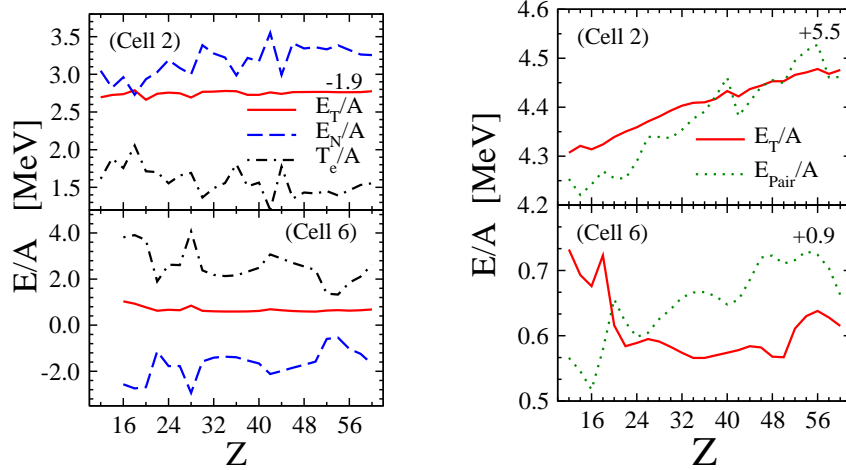
Figure 5. (color online) The different contributions to the total energy in the cells 2 and 6 for the HF (left pannel) and HFB (right pannel) calculations. Are shown: the total energy (solid line), the nuclear energy (dashed line), the kinetic energy of the electrons (dashed-dotted line), and the pairing energy for the ISS pairing interaction (dotted line). The pairing energies are shifted up as indicated in the figure.

calculated inside the cell of radius R_{WS} and employing the same boundary conditions as in HF or HFB calculations. In Ref. [37] it was proposed for the finte size energy correction, Eq. 26, the following parametrisation

$$f(\rho_{n_g}, R_{WS}) = 89.05(\rho_{n_g}/\rho_0)^{0.1425} R_{WS}^{-2} , \qquad (18)$$

where ρ_{n_g} is the average density of neutrons in the gas region extracted from a calculation in which the cell contains both the nuclear cluster and the nonlocalized neutrons while ρ_0 is the nuclear matter saturation density.

How the energy corrections described by Eq. (18) influences the HF (HFB) results can be seen in Fig. 4 (right pannel) and in Table II (last four columns). As expected, the influence of the corrections is more important for the cells 1-5, in which the neutron gas has a higher density, and for those configurations corresponding to small cell radii

4. Effect of pairing on the thermodynamic properties in the inner crust matter

4.1. Specific heat of the baryonic matter

The specific heat of the inner crust has contributions from the electrons, the lattice (or Ion) and the baryonic matter (essentially the de-localized neutrons). The contribution of these 3 components is shown in Fig. 6 where different scenarios for the neutrons are considered. If neutrons are non-superfluid they dominate the contribution of the other component in the inner crust. The effect of the neutron superfluidity is the reduce strongly the contribution of
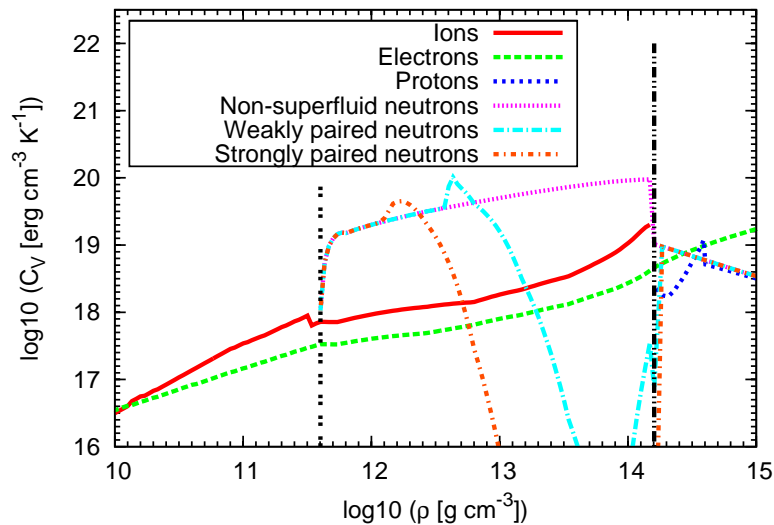
Figure 6. Specific heat in the crust of the neutron star for the different components of the star matter and for a temperature of 10^9 K.

the neutrons. It is therefore expected a very large effect induced by the neutron superfluidity that we now discuss. The specific heat of the neutrons is calculated from the quasiparticle energies obtained solving the HFB equations at finite-temperature in the Wigner-Seitz approximation, as discussed in Section 2.1. For the WS cells we use the structure determined in Ref.[43] (see Table 1).

The specific heat of the neutrons is calculated by

$$C_V = \frac{T}{V}\frac{\partial S}{\partial T},$$ (19)

where V is the volume of the Wigner-Seitz cell, T is the temperature and S is the entropy. The latter is given by

$$S = -k_B \sum_{i,q} g_{i,q}(f_{i,q}\ln f_{i,q} + (1 - f_{i,q})\ln(1 - f_{i,q})).$$ (20)

In Fig. 7 are shown the results obtained for the specific heat in the case of a strong isoscalar pairing interaction. To illustrate the particular behavior of the specific heat in non-uniform matter and the validity of various approximations, in what follows we shall discuss in more detail the results for the cell number 6, which contains N=460 neutrons and Z=40 protons (see Table 1). In this cell the HFB calculations predict 378 unbound neutrons. The specific heat given by the HFB spectrum, in which the contribution of the cluster is included, is shown in Fig. 8 by full line. In the same figure are shown also the specific heats corresponding to two approximations employed in some studies [34, 48, 45]. In these approximations the non-uniform distribution of neutrons is replaced with a uniform gas formed either by the total number of neutrons in the cell (N=460, dashed
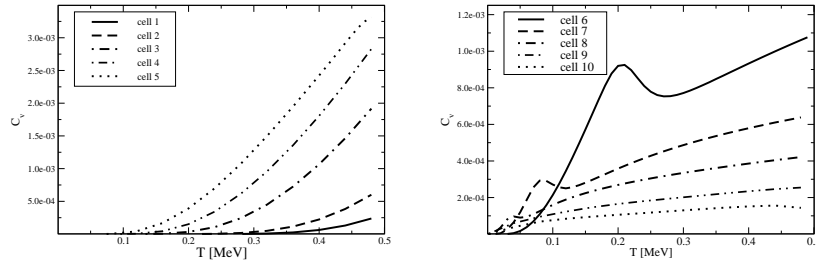
Figure 7. Specific heat of neutrons in various WS cells for isoscalar strong ISS pairing. The specific heat is given in units of Boltzmann constant k_B.
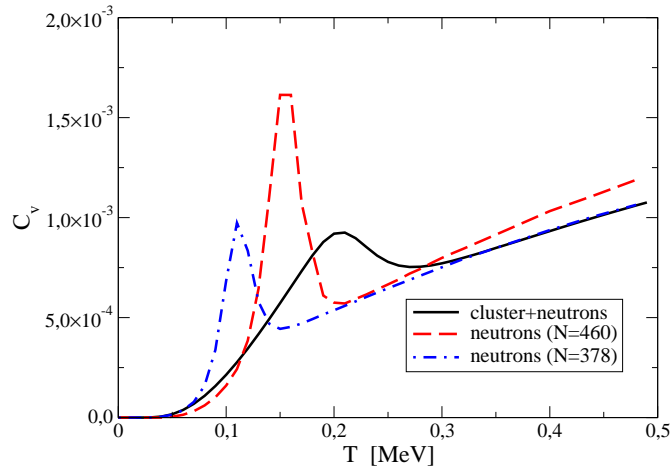

Figure 8. Neutron-specific heat in the the WS cell 6 for isoscalar strong pairing. The results corresponds to various approximations discussed in the paper. The specific heat is given in units of Boltzman constant k_B.

line), or by taking only the number of the unbound neutrons (N=378, dashed-dotted line). How these approximations work is seen in Fig. 8. To make the comparison meaningful, the calculations for the uniform neutron gas are done solving the HFB equations with the same boundary conditions as for the non-uniform system, i.e., neutrons+cluster. As seen in Fig. 8, the transition from the superfluid phase to the normal phase is taking place at a lower temperature in the case of uniform neutron gas, especially when are considered only the unbound neutrons. The critical temperature is therefore lower in uniform matter (for the two prescriptions often used) than in non-uniform matter.

4.2. Pairing and thermalization time of the inner crust

Several studies have shown that the thermalization time depends significantly on the super-fluid properties of the inner crust baryonic matter [34, 25, 48, 40, 54]. This dependence
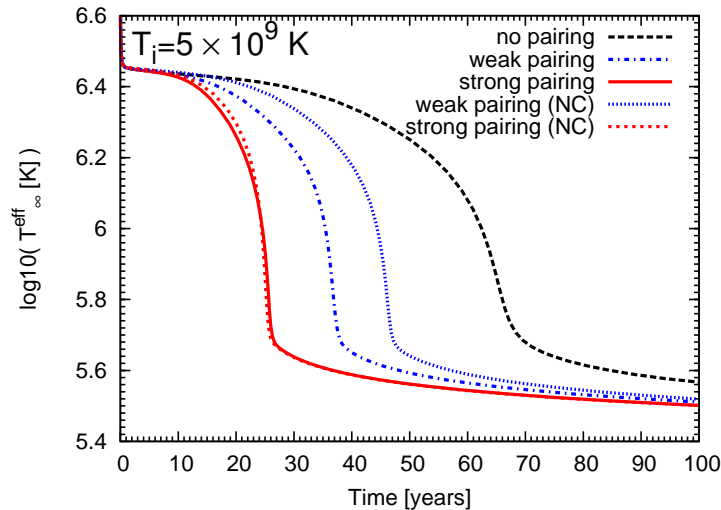
Figure 9. Time evolution of the apparent surface temperature for the initial temperatures $T_i = 500$ keV. NC indicates the results of the calculations obtained by neglecting the effect of the clusters.

is induced through the specific heat of unbound neutrons, strongly affected by the pairing energy gap. As an example we refer to Fig. 6 where it is seen that neutron superfluidity strongly suppress the neutron specific heat which, in the absence of the pairing would dominate over the specific heat of electrons and the lattice.

To estimate the effect of neutron superfluidity to the thermalization time of inner crust matter we use a rapid cooling scenario in which the core arrives quickly to a much smaller temperature than the crust due to the direct URCA colling process. The thermalization time is defined as the time for the core nd the crust temperatures to equilibrate. The heat diffusion is described by the relativistic heat equation [57]:

$$\frac{\partial}{\partial r}\left[\frac{Kr^2}{\Gamma(r)}e^\phi \frac{\partial}{\partial r}(e^\phi T)\right] = r^2 \Gamma(r) e^\phi \left(C_V \frac{\partial T}{\partial t} + e^\phi Q_\nu\right), \tag{21}$$

where t is the time, K is the thermal conductivity, C_V is the specific heat and Q_ν is the neutrino emissivity. The effect of the gravity is given through the gravitational potential ϕ, which enters in the definition of the redshifted temperature $\tilde{T} = Te^\phi$, and the quantity $\Gamma(r) = \left(1 - 2Gm(r)/rc^2\right)^{-1/2}$, where G is the gravitational constant and $m(r)$ is the gravitational mass included in a sphere of radius r. The latter is obtained from the Tolman-Oppenheimer-Volkoff (TOV) equations [29] based on an equation of state obtained from SLy4 Skyrme interaction [20]. More details on the cooling model are given in Ref. [22].

The time evolution of the apparent surface temperature T_∞^{eff} is displayed in Fig. 9 for the initial temperatures of the crust $T_i = 500$ keV [22]. The effective surface temperature shown in Fig. 9 is obtained from the temperature at the bottom of the crust, $T_b = T(\rho_b)$, where $\rho_b = 10^{10}$ g.cm^{-3}, using the relationship given in Ref. [50] for a non-accreted envelope. The results shown in Fig. 9 corresponds to a neutron star of mass 1.6 $M_\odot$ in
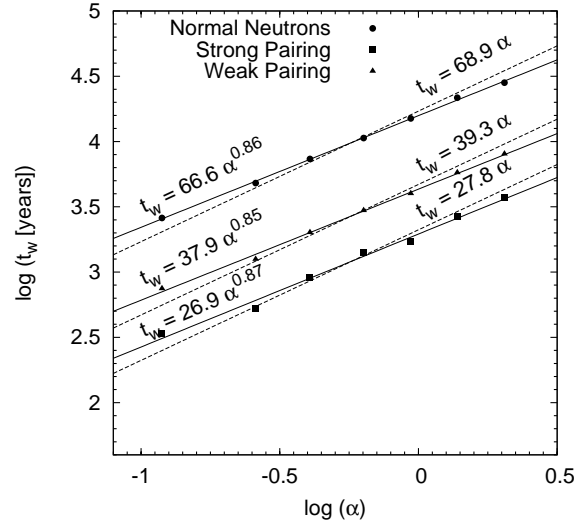
Figure 10. Cooling times t_w versus scaling parameter α for three pairing scenarii as discussed in the text. The results correspond to neutron stars with masses between 1.4 and 2.0 $M_\odot$. The fitting curves are given for the case of a linear scale (dashed lines, right side) and for a fractional power of the scaling parameter α (solid lines, left side).

which the inner crust extends from R_c=10.72 km, which is the radius at the core-crust interface, to 11.19 km. As can be noticed, the pairing enhances significantly the cooling at the surface of the star. In Fig. 9 are also shown the apparent surface temperatures obtained neglecting the effect of the clusters, i.e., supposing that the neutron specific heat is given solely by that of the neutron gas. In this case the neutron specific heat is calculated from the quasiparticle spectrum of BCS equations solved for infinite neutron matter at a density corresponding to that of the external neutrons in the WS cell [35]. In the case of weakly pairing scenario (ISW), the apparent surface temperature is dropping faster for superfluid non uniform matter than for superfluid uniform matter. For the strong pairing scenario, since the pairing correlations suppress the role of the neutron in almost the entire inner crust, the effect of the clusters is less important [22].

A simple random walk model for the cooling is sometimes used to estimate the thermalization time [12, 48, 40]. In this model the diffusion of the cooling wave towards the core is calculated without taking into account the dynamical change of the temperature through the whole crust and neglecting the neutrino emissivity in Eq. (21). The crust is divided into shells of thickness R_i for which the thermal diffusively $D_i = K_i/C_{V,i}$ is considered as constant. From a dimensional analysis of the heat equation (21), the relaxation time of each of these shells is defined as,

$$\tau_i = \Gamma(R)^3 R_i^2/(\gamma D_i), \tag{22}$$

where γ is a geometrical factor and R is the radius of the neutron star. The total relaxation through the crust is given by,

$$\tau_{th} = \left(\sum_i \sqrt{\tau_i}\right)^2. \tag{23}$$

The thermalization time defined as (23) satisfy the condition that in a uniform density case, τ_{th} is independent of the shell discretization. Using this model, the effect of the neutron superfluidity has also been estimated to be large [48, 40], and is qualitatively similar to the result deduced from solving of the heat diffusion equation (21).

In some previous studies [34, 25] it was found that the thermalization time, defined as the time needed for the crust to arrive to the same temperature with the core, satisfies the scaling relation $t_{th} = t_1 \alpha^\beta$ where

$$\alpha = \left(\frac{\Delta R_{\text{crust}}}{1 \text{ km}}\right)^2 \left(1 - 2GM/Rc^2\right)^{-3/2} \tag{24}$$

depends solely on the global properties of the neutron star, i.e., the crust thickness ΔR_{crust}, the star radius R and the mass of the star M. The scaling relation can be inferred from the random walk model presented above. In Fig. 10 are shown as a function of the scaling parameter α the cooling times we have obtained from the solution of the heat diffusion equation (21) for various neutron stars masses lying between 1.4 and 2.0 $M_\odot$ with a step of $0.1 M_\odot$. In this figure are displayed two sets of fits for t_w versus α, i.e., a linear fit with $\beta = 1$ (dashed line) and a fit with a fractional value for β (solid line). It can be noticed that the best fit is obtained with a fractional value for β, which is equal to 0.86 for the normal neutrons, to 0.85 for weakly paired neutrons and to 0.89 for strongly paired neutrons. Considering the simpler linear fit, i.e., $t_w \approx \alpha t_1$, as done in [34, 25], we get for the normalized time t_1 the values $t_1 = \{68.9, 39.3, 22.3\}$ corresponding, respectively, to the normal neutrons, neutrons with weak pairing and neutrons with strong pairing. For a 1.5 $M_\odot$ neutron star with $\alpha = 1.15$, we obtain $t_1 = \{66.4, 37.4, 26.6\}$. These values for t_1 are larger than that of Ref. [25] (Table 2) by a factor 2.3 in the non-superfluid case, and 3.4 (3.0) for the weak (strong) pairing scenario. These differences could be explained by the effects of the nuclear clusters on the neutron specific heat, disregarded in Ref. [25], and by different neutrinos processes and thermal conductivities in the core matter used in the two calculations.

5.   Summary and Conclusions

In the first part of this chapter we have discussed the influence of pairing correlations on the structure of inner crust of neutron stars. The study was done for the region of the inner crust which is supposed to be formed by a lattice of spherical clusters embedded in a gas of neutrons. The lattice was treated as a set of independent cells described in the Wigner-Seitz approximation. To determine the structure of a cell we have used the nuclear binding energy given by the Skyrme-HFB approach. For the cells with high density and small radii the binding energies do not converge to a minimum when the proton number has small values. We believe that it is related to the discretization of the continuum. For a small radius of the cell the average distance between the energy levels of the non-localised neutrons becomes artificially large which cause an underestimation of the binding energy. To correct this drawback we have used an empirical expression based on the comparison between the binding energy of neutrons calculated in infinite matter and in a finite-size spherical cell [37]. We found that the finite size corrections to the binding energies are

significant for the high density cells with small proton numbers. This conclusion indicates the need of a more accurate evaluation of the errors induced by the finite size of the WS cells on nuclear binding energy, which requires to go beyond the empirical expression used here.

In the second part we have discussed how thermalization of neutron stars crust depends on pairing properties and on cluster structure of the inner crust matter. The thermal evolution was obtained by solving the relativistic heat equation with initial conditions specific to a rapid cooling process. The specific heat of neutrons was calculated from the HFB spectrum. The results show that the crust thermalization is strongly influenced by the intensity of pairing correlation. It is also shown that the cluster structure of the inner crust affects significantly the time evolution of the surface temperature.

The thermodynamic properties of the inner crust discussed in this chapter are based on the excitation spectrum of HFB equations. As it was shown in Section 2.2, the QRPA approach predicts in some cells collective excitations located at low energies, comparable with the pairing energy gap. It is thus expected a significant contribution of the collective modes to the specific heat and to the thermalization process of inner crust matter. This is an open issue which deserves further investigations.

References

[1] P. W. Anderson and N. Itoh, Nature 256, 25 (1975).

[2] P. Avogadro, F. Barranco, R. A. Broglia, E. Vigezzi, Nucl. Phys. **A811**, 378 (2008).

[3] M. Baldo, U. Lombardo, E. E. Saperstein, S. V. Tolokonnikov, Nucl. Phys. **A 750**, 409 (2005).

[4] M. Baldo, E. E. Saperstein, S. V. Tolokonnikov, Nucl. Phys. A 775, 235 (2006).

[5] M. Baldo, E. E. Saperstein, and S. V. Tolokonnikov, Eur. Phys. J. A **32**, 97 (2007).

[6] S. Baroni, F. Raimondi, F. Barranco, R.A. Broglia, A. Pastore, E. Vigezzi, arXiv:0805.3962

[7] F. Barranco, R. A. Broglia, H. Esbensen, and E. Vigezzi, Phys. Rev. C **58**, 1257 (1998).

[8] M. Bender, P.-H. Heenen, P.-G. Reinhard, Rev. Mod. Phys. 75, 121 (2003).

[9] G. F. Bertsch and H. Esbensen, Ann. Phys. (N.Y.) **209** 327 (1991).

[10] C. A. Bertulani, H. F. Lü, and H. Sagawa, Phys. Rev. C 80, 027303 (2009).

[11] H. A. Bethe, G. E. Brown, and C. Pethick, Nucl. Phys. **A175**, 225 (1971).

[12] G. E. Brown, K. Kubodera, D. Page, and P. M. Pizzochero, Phys. Rev. D **37**, 2042 (1988).

[13] E. F. Brown, and A. Cumming, Astrophys. J. **698**, 1020 (2009).

[14] L. G. Cao, U. Lombardo, and P. Schuck, Phys. Rev. C 74, 064301 (2006).

[15] E. Chabanat, P. Bonche, P. Haensel, J. Meyer, R. Schaeffer, Nucl. Phys. **A635** 231 (1998) .

[16] N. Chamel, S. Naimi, E. Khan, and J. Margueron, Phys. Rev. **C 75**, 055806 (2007).

[17] N. Chamel, J. Margueron and E. Khan, Phys. Rev. **C 79**, 012801(R) (2009).

[18] N. Chamel, S. Goriely, J. M. Pearson, and M. Onsi, Phys. Rev. **C 81**, 045804 (2010).

[19] J. Dobaczewski, H. Flocard, Treiner, Nucl. Phys A422, 103 (1984).

[20] F. Douchin and P. Haensel, Astron. Astrophys. **380**, 151167 (2001).

[21] S. A. Fayans, S. V. Tolokonnikov, E. L. Trykov, and D. Zaisha, Nucl. Phys. A 676, 49 (2000).

[22] M. Fortin, F. Grill, J. Margueron, D. Page, and N. Sandulescu, Phys. Rev. C (2010).

[23] A. Gezerlis, J. Carlson, Phys. Rev. C81 025803 (2010)

[24] A. L. Goodman, Nucl. Phys. **A352**, 30 (1981).

[25] O. Y. Gnedin, D. G. Yakovlev, A. Y. Potekhin, Mont. Not. R. Astron. Soc. **324**, 725 (2001).

[26] P. Gogelein, and H. Müther, Phys. Rev. C 76, 024312 (2007).

[27] M. Grasso, E. Khan, J. Margueron, N. Van Giai, Nucl. Phys. **A 807**, 1 (2008).

[28] F. Grill, J. Margueron and N. Sandulescu, Submitted to Phys. Rev. C (2011).

[29] P. Haensel, A. Y. Potekhin, D. G. Yakovlev, *Neutron Stars I* (Springer 2007).

[30] K. Hebeler, T. Duguet, T. Lesinski, and A. Schwenk, Phys. Rev. C 80, 044321 (2009).

[31] E. Khan, N. Sandulescu, Nguyen Van Giai, Phys. Rev. C 71, 042801 (2005)

[32] E. Khan, N. Sandulescu, M. Grasso, Nguyen Van Giai, C66 024309 (2002)

[33] L. Landau, Statistical Physics.

[34] J. M. Lattimer et al, ApJ **425** 802 (1994).

[35] K. P. Levenfish, D. G. Yakovlev, Astron. Rep. **38**, 247 (1994).

[36] U. Lombardo and H-J. Schulze, in *Physics of Neutron Star Interiors*, ed. by D.Blaschke et al (Springer, 2001) 30.

[37] J. Margueron, N. Van Giai, N. Sandulescu, Proceeding of the International Symposium EXOCT07, "Exotic States of Nuclear Matter", Edited by U. Lombardo et al., World Scientific (2007); arXiv:0711.0106.

[38] J. Margueron, H. Sagawa, and K. Hagino, Phys. Rev. C76, 064316 (2007).

[39] J. Margueron, H. Sagawa, and K. Hagino, Phys. Rev. C77, 054309 (2008).

[40] C. Monrozeau, J. Margueron, and N. Sandulescu, Phys. Rev. C **75**, 065807 (2007).

[41] J. W. Negele, Phys. Rev. **C 1**, 1260 (1970); X. Campi and D. W. L. Sprung, Nucl. Phys. **A 194**, 401 (1972).

[42] J. W. Negele and D. Vautherin, Phys. Rev. **C 5**, 1472 (1972).

[43] J. W. Negele and D. Vautherin, Nucl. Phys. **A207** 298 (1973).

[44] K. Oyamatsu, Nuclear Physics A561 (1993) 431

[45] D. Page, U. Geppert & F. Weber, Nucl. Phys. **A 777**, p. 497-530 (2006); D. Page & S. Reddy, Annu. Rev. Nucl. & Part. Sci. **56**, 327 (2006).

[46] C. J. Pethick and D. G. Ravenhall, Annu. Rev. Nucl. Part. Sci. **45** 429 (1995).

[47] D. Pines and M. Ali Alpar, Nature (London) **316**, 27 (1985).

[48] P. M. Pizzochero, F. Barranco, E. Vigetti, and R. A. Broglia, ApJ **569**, 381 (2002).

[49] P. M. Pizzochero, arXiv:1105.0156 (astro-ph).

[50] A. Y. Potekhin, G. Chabrier, and D. G. Yakovlev, Astron. Astrophys. **323**, 415 (1997).

[51] N. Sandulescu, L. S. Geng, H. Toki, and G. C. Hillhouse, Phys. Rev. C **68** 054323 (2003).

[52] N. Sandulescu, Nguyen Van Giai, and R. J. Liotta, Phys. Rev. **C69** 045802 (2004).

[53] N. Sandulescu, Phys. Rev. C **70**, 025801 (2004).

[54] N. Sandulescu, Eur. Phys. J. (Special Topics) **156**, 265 (2008).

[55] S. L. Shapiro, S. A. Teukolsky, Black Holes, White Dwarfs, and Neutron Stars, Wiley-VCH editors, 1983.

[56] P. S. Shternin, D. G. Yakovlev, P. Haensel, and A. Y. Potekhin, Mont. Not. R. Astron. Soc. **382**, L43 (2007).

[57] K. S. Thorne, Astrophys. J. 212, 825 (1977).